CONFERENCE PRE-PRINT

IMPACT OF Li-GRANULE INJECTION ON THE IMPROVEMENT OF ENERGY TRANSPORT AND THE EXPULSION OF IMPURITIES IN THE LHD HELIOTRON

D. MEDINA-ROQUE Laboratorio Nacional de Fusión, CIEMAT Madrid, Spain Email: daniel.medina@ciemat.es

¹KIERAN J. MCCARTHY, ²NAOKI TAMURA, ¹ISABEL GARCÍA-CORTÉS, ^{3,4}KENJI TANAKA, ⁵FEDERICO NESPOLI, ^{3,6}MAMORU SHOJI, ^{3,6}SUGURU MASUZAKI, ³HISAMICHI FUNABA, ^{3,6}CHIHIRO SUZUKI, ⁷ALBERT MOLLÉN, ⁵ROBERT LUNSFORD, ³KATSUMI IDA, ³MIKIRO YOSHINUMA, ^{3,6}MOTOSHI GOTO, ^{3,6}YASUKO KAWAMOTO, ^{3,6}TOMOKO KAWATE, ^{3,6}TOKIHIKO TOKUZAWA, ^{3,6}ICHIHIRO YAMADA and the ³LHD EXPERIMENTAL TEAM.

Abstract

This work shows how continuous lithium (Li) granule injection into high-density stellarator plasmas can enhance core impurity transport. This technique improves energy confinement by reducing turbulence and simultaneously increases the transport of mid- and high-Z impurities. STRAHL code predictions indicate that the convection and diffusion coefficients for such impurities have square-root dependences on charge and that the diffusion is 4-5 times higher than the neoclassical predictions, findings that point towards a combination of collisional and turbulence effects of the observed enhanced impurity transport. In parallel, the levels of intrinsic impurities reduce slightly, possibly due to a combination of a conditioning effect from cumulative Li deposition on the vacuum vessel walls and an increase of collisional transport. A positive radial electric field is measured in the Scrape-Off Layer (SOL) that doubles with Li injection, while a negative one, that seems unaffected by the presence of Li, is measured inside the plasma. Neoclassical transport is expected to be the dominant factor for the primary plasma components (electrons, ions and low-charge impurities) and SFINCS drift-kinetic transport code simulations shows that their particle fluxes are increased during Li injection. In contrast, the same simulations indicate that the classical contribution becomes more significant for high-Z impurity transport and it significantly increases in the presence of Li. In particular, this study highlights experimental evidence that indicates that classical transport can play a crucial role in enhancing the transport of high-Z impurities in high-density stellarator plasmas, a condition made possible by continuous Li-granule injection. This method can be an effective real-time technique for removing core and edge impurities and for improving overall plasma performance.

1. INTRODUCTION

A major challenge for the development of stellarator-based fusion reactors is establishing operational conditions that sustain long-duration confinement of bulk particles and energy, concurrently while mitigating impurity accumulation, especially of high-Z elements which can lead to plasma radiative collapse [1]. This issue is particularly pronounced in high-density plasma regimes, where an inward-pointing ambipolar radial electric field (ion-root) extends confinement and reduces diffusive impurity transport [2, 3]. Whilst the suppression of anomalous transport, often driven by plasma turbulence, is a common strategy to improve fuel particle confinement [4], it can paradoxically enhance impurity confinement, a phenomenon observed experimentally and corroborated by neoclassical (NC) simulations [1]. Prior investigations on the Large Helical Device (LHD) identified an "impurity hole" (a highly hollow impurity profile) in low-density, high-ion-temperature plasmas, prompting extensive studies into their NC and anomalous transport characteristics [5]. Although Ion Temperature Gradient (ITG) turbulence drives inward impurity fluxes [6], detailed NC simulations have highlighted the critical role of thermo-diffusion in facilitating outward impurity fluxes. In high-density LHD plasmas, supplementary electron cyclotron resonance heating (ECRH) has been shown to aid in expelling impurities exclusively from the core region [7], though the underlying mechanisms remain largely unexplained. Recently, a reduced-turbulence scenario with enhanced impurity transport was achieved experimentally, for the first time, by the injection of Ligranule dropping in LHD [8]. Such experiments employed Tracer-Encapsulated Solid Pellet (TESPEL) injections

¹Laboratorio Nacional de Fusión, CIEMAT, Madrid, Spain

²Max-Planck Institute for Plasma Physics, Greifswald, Germany

³National Institute for Fusion Science, National Institutes of Natural Science, Toki, Japan

⁴Interdisciplinary Graduate School of Engineering Sciences, Kyushu University, Kasuga, Japan

⁵Princeton Plasma Physics Laboratory, Princeton, NJ, USA

⁶The Graduate University of Advanced Studies, SOKENDAI, Toki, Japan

⁷Department of Electrical Engineering, Royal Institute of Technology, Stockholm, Sweden

[9] into high-density, low-ion-temperature LHD plasmas, to investigate core impurity transport in this new scenario. Continuous Li-granule injection was observed to improve plasma performance, consistent with findings from dropping other low-Z (B, BN, or C) powders [10-12]. However, unexpectedly, a distinct reduction in the confinement time of mid/high-Z tracers injected with TESPEL was noted upon Li-granule introduction. This paper delves deeper into physical mechanisms that could explain the experimental observations reported in [8]. First, the effects of Li-injection on overall plasma performance are reviewed, in particular an observed improvement in energy confinement time, this being compared with previous results obtained with B-injection [10]. Second, the enhancement of mid/high-Z core impurity transport is reviewed. Next, the effect of Li-injection on intrinsic impurity levels is compared with levels for previous B-injections [11]. Finally, changes in the radial electric field, E_r, and plasma turbulence induced by Li are presented in detail and simulations performed with SFINCS and STRAHL codes provide potential physical explanations for experimental observations.

2. EXPERIMENTAL SET-UP

The experiments reported here were conducted in the LHD, which is the largest superconducting heliotron-type device, featuring a major radius of 3.9 m, a minor radius of 0.6 m, and a typical plasma volume of 30 m³ [13]. A

comprehensive suite of diagnostics is employed [14], including Charge-Exchange recombination Spectroscopy (CXS), 2dimensional Phase Contrast Imaging (2D-PCI), visible Bremsstrahlung measurement, Vacuum and Extreme Ultraviolet (VUV/EUV) spectroscopy, and Doppler Reflectometry. The LHD is equipped with an Impurity Powder Dropper for injecting submillimeter impurity grains via gravity [15]. TESPELs, which allow the precise introduction of known tracer quantities at predetermined radii and times, are used [9]. Titanium (Ti) and molybdenum (Mo) are selected as tracers. Experiments were carried out in an inward-shifted magnetic configuration with a vacuum magnetic axis position at $R_{ax} = 3.6$ m and a magnetic field strength at the magnetic axis of $B_{ax} = 2.75$ T. Hydrogen (H₂) gas served as the working gas. The heating scheme involved 3 MW of ECRH power from 3 s to 5 s, 3 MW of tangential NBI from 3.3 s to 5 s (increased to 7 MW from 5 s to 7 s), and 4 MW of perpendicular modulated NBI for CXS from 5 s to 7 s.

EXPERIMENTAL RESULTS

3.1. Plasma performance

A series of discharges with Li-granule dropping was performed in LHD to characterize this operational scenario and to study impurity confinement. Plasma parameters for reference discharges (without Li-granules) are line-averaged density, $n_{e,avg}$, ~5.3 x 10^{19} m⁻³, a central electron temperature, $T_{\text{e,0,}}$ ~2.4 keV, and a diamagnetic energy, W_p, ~880 kJ. See Fig. 1. In discharges with continuous Ligranules, dropping occurs from ~4.8 s until discharge end, this being identified by Li I emissions (see Fig. 1e). Comparing discharges with and without Li-granule dropping shows several modifications to plasma parameters. For instance, increases are seen in $n_{e,avg}(\Delta n_{e,avg}/n_{e,avg} < 5\%)$, $T_{e0}(\Delta T_{e0}/T_{e0} \sim 12.5\%)$ and plasma stored energy ($\Delta W_p/W_p \sim \! 10\%$) while Z_{eff} rises from ~1.8 to ~2.3. Furthermore, a close to 25% reduction in Hα emission is observed, suggesting a potential decrease in particle fueling despite an almost constant line-averaged electron density, a finding that may indicate improved bulk-ion particle confinement.

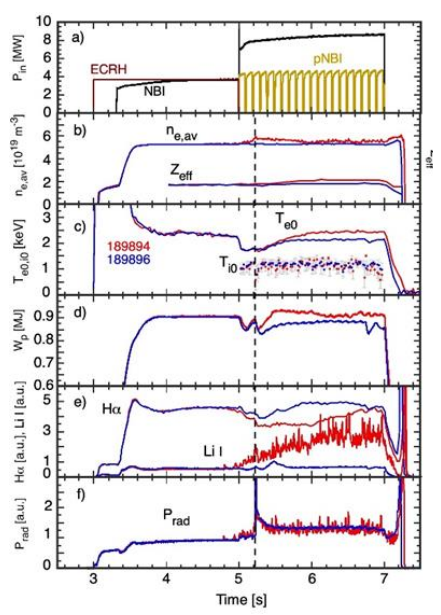


FIG 1. Traces for a) electron cyclotron resonance heating (ECRH), tangential neutral beam injection (NBI), and perpendicular neutral beam diagnostic (pNBI); b) line-averaged electron density (n_{e,avg}) and effective charge (Z_{eff}) (from 4 s to 7.2 s for clarity); c) central electron (T_e) and ion (Ti) temperature; d) stored plasma energy (transient NBI malfunctions cause brief signal drops); e) Li I (670.8 nm) and Balmer Hα (656.3 nm) intensities; and f) total radiated power (P_{rad}) for #189896 (reference discharge without lithium granules but with Mo TESPEL injection blue) and #189894 (continuous lithium granules and Mo TESPEL injection - red), TESPEL injections are indicated by a vertical dash-dash line at 5.225 s.

It is seen also that the introduction of Li-granules alters plasma profile shapes. For instance, as depicted in Fig. 2, the electron density (ne) increases in the outer plasma region (where normalized effective minor radius, $r_{eff/a99}$, is between 0.7 and 1), while remaining stable in the core ($r_{eff/a99} < 0.7$). Here, r_{eff} represents the effective minor radius, and agg is the minor radius within which 99% of the total plasma stored energy is contained. This increase in edge density results in a slightly hollower density profile. Furthermore, both the central electron temperature (T_e) and ion temperature (T_i) are seen to rise when Li-granules are introduced, the latter despite significant error bars. Lastly, while the inverse scale lengths of n_e and T_e appear nearly identical in both scenarios (with and without Li-granules), the inverse scale length of T_i seems to increase during Li-granule dropping in the region $r_{eff/a99} > 0.8$. All these measurements point towards a significant improvement in plasma performance since, for the same heating power and line-averaged electron density, substantial steepening of electron and ion temperature profiles are achieved.

FIG 2. Radial profiles of electron a) density and b) temperature, and c) ion temperature at \sim 6 s for discharges #189896 (without lithium granules - blue) and #189894 (with lithium granules - red). Attenuation of the pNBI beam limits reliable ion temperature measurements to $r_{\rm eff/a99} > 0.2$. In both cases, a Mo-TESPEL is injected at t = 5.225 s.

3.2. Energy confinement

Plasma confinement during Li-granule dropping is compared here with predictions from the ISS04 scaling law [16]. For this, the energy confinement time is evaluated from the W_p traces of Fig. 1 as $\tau^E = W_p/(P_{abs} - dW_p/dt)$. From neutral beam injected power, P_{in} , the absorbed power, P_{abs} , is estimated as $P_{abs} = P_{in} [1 - \exp(-\sigma n_{e,av} l)]$, where $\sigma = 0.43$ is the effective cross-section for neutral beam ionization in a H plasma and l = 1.86 m is beam absorption length [17]. τ^E values for selected discharges are plotted in Fig. 3 against ISS04-based scaling law

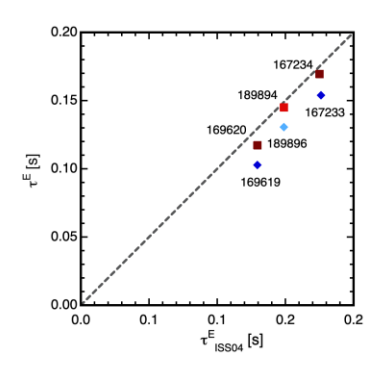


FIG 3: Experimental energy confinement times, t^E , versus ISS04-based scaling law predictions, τ^E_{ISS04} , [26] for selected discharges with/without Li- or B-granule dropping. They are for #189894 (Li-granules, red square), #189896 (reference, sky blue diamond), #169620 and #167234 (B-granules, dark red squares), and #169619 and #167233 (reference, navy blue diamonds). All discharges were made in the inward-shifted magnetic configuration with $R_{ax} = 3.68$ m, $B_{ax} = 2.75$ T, a = 0.63 m and $t_{2/3} = 0.65$. For B-granules, $n_e = 3$ x 10^{19} and 3.2 x 10^{19} m⁻³ and $P_{in} = 3.5$ and 6 MW, respectively. For Li-granules, $n_e = 5.3$ x 10^{19} m⁻³ and $P_{in} = 7$ MW.

predictions, τ^E_{ISS04} , [16] for discharges with/without Li- or B-granule dropping. It is seen that τ^E / τ^E_{ISS04} increases for Li-granule injection, this increase being ~15% when compared to a reference shot. Similar increases were obtained, albeit for lower electron densities, for previous B-granule injections when compared to reference shots [10]. In Fig. 3, all reference τ^E values are significantly lower than ISS04 predictions, low-Z granule dropping results in consistent increases in τ^E .

3.3. Impurity confinement

In order to assess the impact of Li-granules on impurity confinement, impurity tracers are injected in Fig. 1 using the TESPEL method at $t=5.225~\rm s$, (TESPEL injections were not made during B-injection). Next, to investigate any potential atomic number dependence, Titanium (Ti, Z=22) and Molybdenum (Mo, Z=42) are used. The quantities of injected Ti and Mo are 2.94×10^{17} Ti atoms for discharge #189891, 2.82×10^{17} Ti atoms for #189893, 4.98×10^{17} Mo atoms for #189894, and 5.92×10^{17} Mo atoms for #189896. The estimated deposition location for these impurities is at

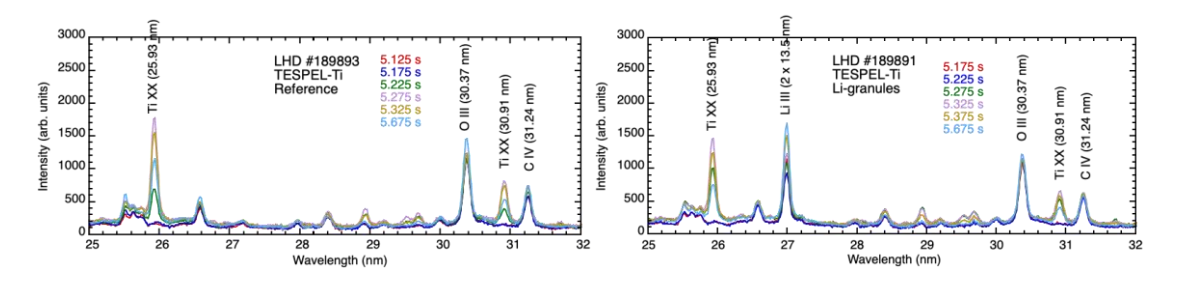


FIG 4: EUV spectra collected at various times along LHD discharges #189893 (reference) and #189891(Li-granule dropping) before and after a TESPEL-Ti injection at 5.225 s. Identified emission lines of Ti, Li, C and O are highlighted [18].

a normalized effective radius of $r_{eff/a99} \approx 0.75$, which corresponds to the density profile shoulder. Typically, TESPEL injections cause a minor, transient increase in n_{e,avg}, a 5% decrease in W_p (which recovers fully within 200 ms), and a ~ 50% reduction in T_i (which recovers after approximately 50 ms). With regard to tracer line emissions, Fig. 4 shows examples of EUV spectra, measured by the SOXMOS spectrometer [19], for discharges with a TESPEL-Ti injection. From these spectra, it is found that the intensity of the Ti XX emission line at 25.93 nm decreases more rapidly when Li-granule injection is performed, this indicating enhanced impurity removal. A similar trend is observed for the Mo XXXII (12.79 nm) emission line when TESPEL-Mo injections are performed in reference and Ligranule discharges. For this, the temporal evolution of specific charge states is determined by integrating the areas under such emission lines, after accounting for background continuum. See Fig. 5. In this way, the confinement times for Ti is found to be 1.38 s without Li-granules and 1.15 s with Li-granules, a reduction of approximately 17%. For Mo, the confinement time without Li-granules is 6.34 s, this decreasing dramatically to 1.43 s for Li-granules, a reduction of ~78%. These results suggest that, in plasmas with continuous Li-granule injection, impurity confinement time reduction is more pronounced for high atomic number impurities.

In addition to tracers, intrinsic impurities are monitored also using VUV spectroscopy. For example, the evolution of carbon (C III at 97.7 nm), oxygen (O V at 63 nm) and iron (Fe XVI at 33.5 nm) along selected discharges are shown in Fig. 6. Here, the C III signal, normalized to $n_{e,avg}$, is reduced by ~30% during Ligranule injection, the O V trace is reduced slightly, whereas the Fe XVI signal appears to be unaffected by the Li. This contrasts with previous observations made with B-granule dropping in LHD, in which the conditioning effect was more effective and O and Fe levels were more strongly damped than those of C [11]. Now, comparing #189885 and #189894, discharges with similar Li-granule injection rates and plasma parameters, the former being made at the start of the experimental session and the latter being made after several discharges with Li-granule dropping, there seems to be a very slight cumulative effect due to Li deposition on the first wall that leads to reduced levels of intrinsic impurities in subsequent discharges.

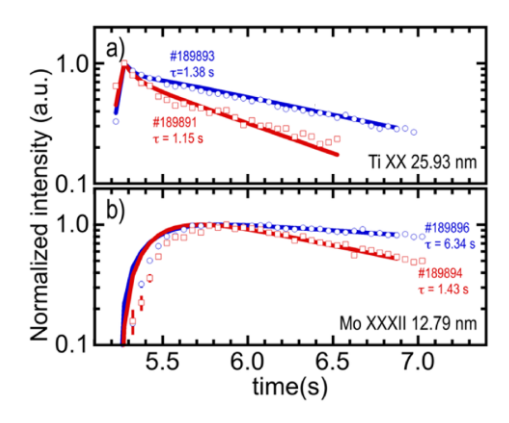


FIG. 5: Semi-logarithmic plots of normalized intensities for a) Ti XX and b) Mo XXXII emission lines. Open points are experimental values whilst solid lines represent STRAHL predictions. Data is presented for discharges #189893 and #189896 (without lithium granules - blue) and #189891 and #189894 (with Ligranules - red). TESPELs are injected at 5.225 s.

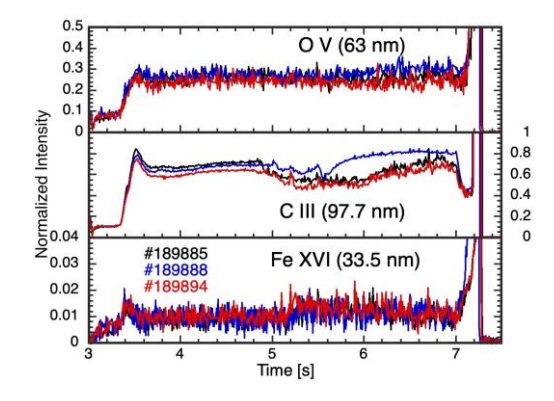


FIG 6: Temporal evolution of O V, C III and Fe XVI spectral lines (intensities normalized by line-integrated density) for discharges #189888 (no Lipowder, blue), #189885 (Li-powder, black) and #189894 (Li-powder, Mo-TESPEL, red).

3.4. Radial electric field

It is critical to understand how Li-granule dropping affects impurity transport in the region where $r_{eff/a99}>0.6$. Firstly, the radial electric field, E_r , is considered a key factor for impurity transport in high-density LHD plasmas

[20]. However, at high densities, the CXS diagnostic can only estimate E_r in the region where $r_{eff/a99}>0.8$ due to significant attenuation of the probe neutral beam. In the discharges studied here, E_r values determined from CXS show similar negative magnitudes regardless of whether Li-granules are present or absent, see Fig. 7 a). In contrast, a positive E_r is measured by a Doppler Reflectometer (DR) in the Scrape-Off Layer (SOL), see Fig. 7 b), that becomes 2 times more positive in the presence of Li-granules. This increase may be directly affecting the transport of intrinsic impurities, which originate from plasma-wall interactions and enter the plasma through the SOL, by enhancing the outward neoclassical transport expected in presence of a positive radial electric field. However, its implication for the enhanced decay of TESPEL tracers is not straight-forward as these are deposited deeper inside the plasma. Moreover, the level of C²⁺, which is assumed to reside in the outermost plasma edge due to its low ionization energy (47.89 eV), appears to recover as the positive E_r reduces these. This might indicate that, as well as improved wall conditioning, changes in collisional impurity transport are driving the reduction of this intrinsic impurity

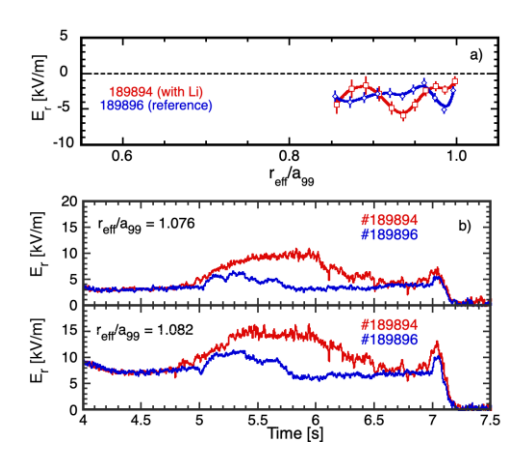


FIG 7: a) E_r measured by CXS at 6.39 s for $r_{eff}/a_{99} > 0.8$ and b) the temporal evolution of E_r at two radial positions in the SOL as measured by a DR system [21] for #189894 (Li-powder from ~4.8 s, red) and #189896 (reference, blue).

ion. In contrast, O V and Fe XVI have much higher ionization energies so O^{4+} and Fe^{15+} reside deeper inside the plasma, thus they might be less affected by the positive E_r in the SOL.

3.5. Turbulence

To examine how Li-granule injection affects plasma turbulence, signals from a 2D-PCI diagnostic measures ion-scale turbulence with wavenumbers (k) ranging from 0.1 to 0.8 mm⁻¹ and frequencies (f) from 20 to 500 kHz are considered. As seen in Fig. 8a), the temporal evolution of local fluctuation amplitudes at $r_{eff/a99}$ =0.8 indicates that turbulence is reduced during Li- granule dropping. This is further supported by density fluctuation spectrograms in Figs. 8b) and 8c) that show reduced turbulence across the whole plasma cross-section for $r_{eff/a99}$ >0.4. The time-averaged spectra in Fig. 8d) reveal that fluctuations in the frequency range of $5 \le f \le 500$ kHz are significantly suppressed (by nearly an order of magnitude in the range of a few tens of kHz) by Li-granules. The turbulence reduction appears to be broader than what typically observed in previous B powder injection experiments, nevertheless consistent with the observed trend of stronger turbulence reduction for higher plasma densities [12]. In this context, the dominant turbulence is likely to be Resistive Interchange (RI) turbulence [21], as Ion Temperature Gradient (ITG) turbulence is presumed to be stable given its instability threshold of an inverse scale length of Ti (L_{Ti}^{-1}) of approximately 2.5 m⁻¹ [22]. In addition, the radial profile of the fluctuation amplitude, as shown in Fig. 8e), was also reduced by a factor of two in discharge #189894. Although reduced RI turbulence

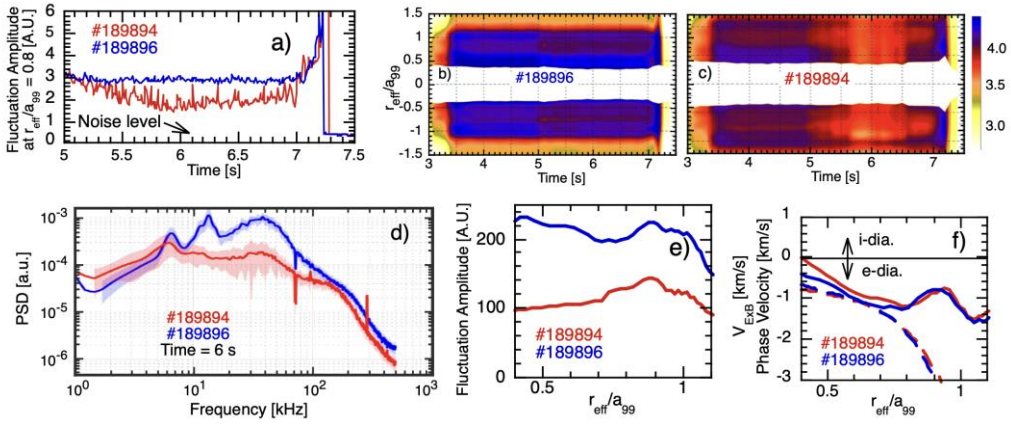


FIG 8. For discharges #189894 (with Li-granule dropping - red) and #189896 (without Li-granules - blue). a) Fluctuation amplitude temporal history at $r_{eff/a99} = 0.8$, b) and c) spectrograms of line-integrated phase-contrast imaging signals, d) comparison of turbulence power spectral density (PSD), the shaded areas representing standard deviation, plus radial profiles of e) fluctuation amplitude and f) fluctuation phase at 6 s (continuous), estimated using 2D-Phase Contrast Imaging. Also shown in f) are ExB velocities (V_{ExB}) estimated by SFINCS (dash-dash).

offers a potential explanation for improved energy confinement, it is improbable that it promotes impurity removal. On the contrary, the effect would be expected to be detrimental. Finally, Fig. 8f) displays fluctuation phase velocities in the laboratory frame, where poloidal components are the main contributors to the measured wavenumber components. These phase velocities are therefore considered a good approximation of the E×B poloidal rotation velocities. The E_r values inferred from these phase velocities is found to be negative and nearly identical both with and without Li-granules. Figure 8f) also includes E×B velocities, $V_{E\times B}$, predicted by the collisional transport code SFINCS [23] for both cases, which is consistent with the 2D-PCI measurements in the range of $0.4 < r_{eff/a99} < 0.7$. Furthermore, the $V_{E\times B}$ predicted by SFINCS is also nearly identical in this region, regardless of whether Li-granules were present or absent.

4. SIMULATIONS

4.1. Collisional particle fluxes computed by SFINCS

In order to shed light on the underlying physics, a comparison is made between the classical and neoclassical (NC) particle fluxes predicted by the SFINCS code [23] for plasmas with and without lithium granule dropping. As seen in Fig. 9 a) and b), the total electron and proton particle fluxes are driven primarily by the NC contribution and increase when Li-granules are introduced (shot #189894). In addition, both electron and ion heat fluxes increase during Li-injection, this being consistent with previous results with B-injection [10]. A possible explanation is that, as turbulent transport is reduced, a steepening of the temperature profiles increases neoclassical transport and the increased outward NC particle fluxes generate the observed shoulder in the hollower electron density profile. In the simulations, an "average" impurity ion charge of ~3.5 is used to represent He, Li, and C. For simplicity, the shape of the averaged impurity density profile is assumed to be identical to that of the electron density. This approach reduces simulation costs while providing consistent results for bulk particle fluxes and the E_r, which is negative across the whole plasma cross section due to the NC ion-root present at high electron densities and which becomes slightly more positive at the plasma edge during Li-powder injection, see Fig. 9 e). The NC fluxes, which are dominant for this averaged impurity, are found to become more negative with the addition of lithium across all radii, in order to maintain ambipolarity. As postulated recently, such enhanced inward-directed NC fluxes could increase the impurity density gradient in the plasma core, a process that may also contribute to a reduction in core turbulence [24]. In

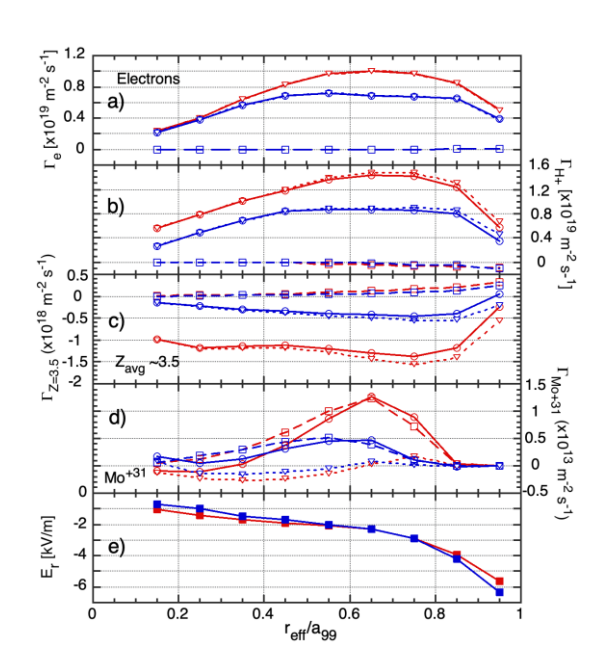


FIG 9. Neoclassical (NC) (open circles, long dashdash), classical (squares, short dash-dash), and total (open triangles, continuous) particle fluxes normalized to pseudo-densities for a) electrons, b) H^+ ions, c) effective impurity contents with average charge (Z_{avg}) of ~3.5, and d) trace Mo^{31+} ions as functions of normalized minor radius, plus e) estimated E_r profiles. Predictions are generated using the SFINCS code for discharges #189894 (left, with Li-granules - red) and #189896 (right, without Li-granule - blue).

the case of an injected tracer, the Mo³¹⁺ particle fluxes are directed outwards generally and are governed predominantly by the classical contribution across all radii in discharges without Li, e.g., #189896. These fluxes become significantly more positive outside of r_{eff/a99}≈0.45 when Li is injected, e.g., #189894. For this, the Mo³¹⁺ ion density is kept at a trace level in the simulation, which assumes coronal equilibrium, in order to avoid altering significantly the average charge (Z_{avg}). Similar results are obtained when a Gaussian density profile, centred around the expected deposition location, is assumed for Mo. Further details on these SFINCS results and additional simulations will be presented in a separate paper. The experimental findings here are consistent with prior simulation-based predictions for impurity transport [25], which found that classical transport can exceed the NC contribution for mid-Z species in the NC-optimized stellarator W7-X. While classical transport is generally been considered negligible when compared to other transport channels (NC and turbulent), these findings provide experimental evidence that it can be a critical factor for core impurity transport under specific plasma conditions. This is particularly so if Li-granules are dropped into the plasma edge when NC inward and outward fluxes are nearly balanced.

4.2. Comparison of transport coefficients predicted by STRAHL and SFINCS

Simulations are conducted here using the STRAHL impurity transport code [26], assuming radially uniform diffusion coefficients, D, with results shown in solid lines in Fig. 5. The temporal evolution of Ti XX emissions without Li-granules is reproduced accurately for a diffusion coefficient of $D = 0.11 \text{ m}^2/\text{s}$ and the convection velocity (V) profile, which has a minimum of V = -1.55 m/s. With the introduction of Li- granules, the same D and a slightly narrower negative V profile (with minimum of V = -0.95 m/s), it is possible to replicate the observed

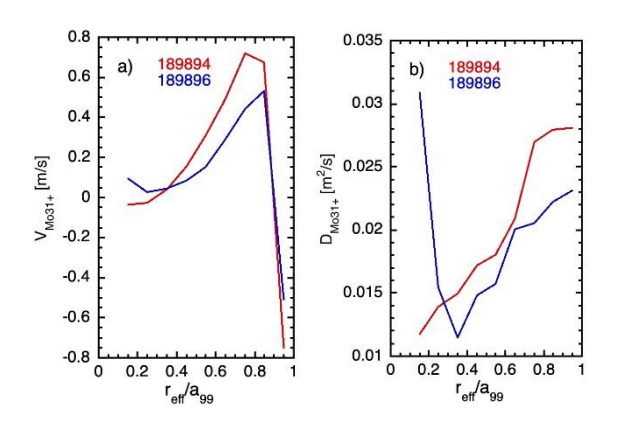


FIG 10. Convective velocity and diffusion coefficient profiles predicted by SFINCS for discharges #189894 (with Li- granules - red) and #189896 (without Li-granules - blue).

that a square-root dependence on charge could also reproduce the decay phase temporal evolutions of Mo XXXII emissions. This suggests that the D for Mo is approximately $0.085 \text{ m}^2/\text{s}$, (calculated as $0.11 \text{ m}^2/\text{s} \times \sqrt{Z_{Ti^{19}} + /Z_{Mo^{31+}}}$), while V is around -2.0 m/s without Li and -1.2 m/s with Li, based on similar scaling [8]. This dependency on the square root of charge states suggests that the observed enhanced impurity transport may be linked a combination of collisional and turbulence effects, in contrast with the direct dependence of V on the charge for mid-Z impurities in scenarios without Li-injection and the subsequent reduced-turbulence [27]. A comparison with predictions from the SFINCS collisional transport code revealed several differences. For instance, the D

from SFINCS (Fig. 10) is 4 to 5 times smaller than the STRAHL estimate indicating that, despite being

temporal evolution of Ti XX. Further analysis shows

significantly reduced, it still plays an important role in the impurity transport. Although the V from SFINCS has an opposite sign to the STRAHL result, both simulations indicate that it becomes more positive with Li injection (see Fig. 10). This supports a reduced inward pinch for plasmas with Li granule dropping. STRAHL results also suggest that the impact of Li-granule dropping on core impurity transport is consistent for both Ti and Mo.

5. SUMMARY

In summary, continuous dropping of Li-granules into high-density LHD plasmas leads to several key outcomes: improved energy confinement, enhanced core transport of mid/high-Z impurities, and reduced levels of intrinsic impurities. Also, it is found that E_r becomes more positive in the SOL but remains negative and similar to preinjection conditions inside the plasma. Simulations with the STRAHL and SFINCS codes indicate that classical transport is the primary mechanism enhancing core impurity transport in the r_{eff/a99}>0.6 region when Li-granules are introduced. While classical transport has been considered relevant for mid-Z impurities in the NC-optimized W7-X stellarator [25], these results indicate that this mechanism can also be significant in non-NC-optimized devices such as LHD under specific plasma conditions. These conditions are characterized by a minimized NC transport channel, where NC inward and outward fluxes are nearly balanced. Such a condition might be achieved in tokamak plasmas also, such as in ITER, since classical transport depends only on collisions rather than on magnetic configuration, however, this requires future simulations and experiments. These findings are critical for the development of future fusion devices where impurity accumulation is a major concern. The impurity powderdropping method is now a promising real-time wall conditioning technique also. Our results seem to demonstrate that Li granule dropping may not only improve overall plasma performance, as already shown in previous publications [10-12], but can also flush out core impurities effectively, providing a viable strategy for impurity control in next-generation fusion reactors..

ACKNOWLEDGEMENTS

This work has been carried out within the framework of the EUROfusion Consortium, funded by the European Union via the Euratom Research and Training Programme (Grant Agreement No 101052200 - EUROfusion). Views and opinions expressed are however those of the author(s) only and do not necessarily reflect those of the European Union or the European Commission. Neither the European Union nor the European Commission can be held responsible for them. It is partially financed by grants PID2020-116599RB-I00 and PID2023-148697OB-I00 funded by MCIN/AEI/10.13039/501100011-033 and by ERDF, A Way of Making Europe. It is partially supported also by the U.S. DOE under Contract No. DE-AC02-09CH11466 with Princeton University, by JSPS

KAKENHI JP23KK0054 and by NIFS grant administrative budgets (10203010LHD105 and 10201010PSU003). Computing resources were provided on the computer Stellar operated by the Princeton Plasma Physics Laboratory and Princeton Institute for Computational Science and Engineering.

REFERENCES

- [1] MAAßBERG, H. et al., Density control problems in large stellarators with neoclassical transport, Plasma Phys. Control. Fusion 41 (1999) 1135.
- [2] SUDO S., A review of impurity transport characteristics in the LHD, Plasma Phys. Control. Fusion 58 (2016) 043001.
- [3] BURHENN R. et al., On impurity handling in high performance stellarator/heliotron plasmas, Nucl. Fusion 49 (2009) 065005.
- [4] TANAKA K. et al. Particle Transport of LHD, Fusion Sci. Tech. 58 (2010) 70.
- [5] IDA K. et al., Observation of an impurity hole in a plasma with an ion internal transport barrier in the Large Helical Device, Phys. Plasmas 16 (2009) 056111.
- [6] TANAKA K. et al., Turbulence Response in the High Ti Discharge of the LHD, Plasma Fusion Res. 5 (2010) S2053.
- [7] TAMURA N. et al., Observation of the ECH effect on the impurity accumulation in the LHD, Phys. Plasmas 24, (2017) 056118.
- [8] MEDINA-ROQUE D. et al., Observation of Enhanced Core Impurity Transport in a Reduced-turbulence Stellarator Plasma, submitted to Phys. Rev. Lett. (2025).
- [9] SUDO S. and TAMURA N., Tracer-encapsulated solid pellet injection system, Rev. Sci. Instrum. 83 (2012) 023503.
- [10] NESPOLI F. et al., Observation of a reduced-turbulence regime with boron powder injection in a stellarator, Nat. Phys. 18 (2022) 350.
- [11] LUNSFORD R. et al., Real-time wall conditioning and recycling modification utilizing boron and boron nitride powder injections into the Large Helical Device, Nucl. Fusion 62 (2022) 086021.
- [12] NESPOLI F. et al., A reduced-turbulence regime in the Large Helical Device upon injection of low-Z materials powders, Nucl. Fusion 63 (2023) 076001.
- [13] IIYOSHI A. et al., An Overview of the Large Helical Device Project, Fusion Tech. 17 (1990) 169.
- [14] KAWAHATA K. et al., Overview of LHD Plasma Diagnostics, Fusion Sci. Tech. 58 (2010) 331.
- [15] NAGY A. et al., A multi-species powder dropper for magnetic fusion applications, Rev. Sci. Instrum. 89 (2018) 10K121.
- [16] YAMADA H. et al., Characterization of energy confinement in net-current free plasmas using the extended International Stellarator Database, Nucl. Fusion 45 (2005) 1684.
- [17] TAKEIRI Y. et al., High-ion temperature experiments with negative-ion-based neutral beam injection heating in Large Helical Device. Nucl. Fusion 45 (2005) 565-
- [18] KRAMIDA A. et al., NIST Atomic Spectra Database (ver. 5.12) (2024), https://physics.nist.gov/asd.
- [19] SCHWOB J. L. et al., High-resolution duo-multichannel soft x-ray spectrometer for tokamak plasma diagnostics, Rev. Sci. Intrum. 58 (1987) 1601.
- [20] VELASCO J. L. et al., Large tangential electric fields in plasmas close to temperature screening, Plasma Phys. Control. Fusion 60 (2018) 074004.
- [21] KINOSHITA T. et al., Turbulence Transition in Magnetically Confined Hydrogen and Deuterium Plasmas, Phys. Rev. Lett. 132 (2024) 235101.
- [22] TANAKA K. et al., Collisionality dependence and ion species effects on heat transport in He and H plasma, and the role of ion scale turbulence in LHD, Nucl. Fusion 57 (2017) 116005.
- [23] LANDREMAN M. et al., Comparison of particle trajectories and collision operators for collisional transport in nonaxisymmetric plasmas, Phys. Plasmas 21 (2014) 042503.
- [24] GARCÍA-REGAÑA J.M et al., Phys. Rev. Lett. 133 (2024) 105101.
- [25] BULLER S.et al., The importance of the classical channel in the impurity transport of optimized stellarators, J. Plasma Phys. 85 (2019) 175850401.
- [26] BERHINGER K., Description of the impurity transport code 'STRAHL', JET Report (1987) JET-R (87) 08.
- [27] NOZATO H. et al., A study of charge dependence of particle transport using impurity pellet injection and high-spatial resolution bremsstrahlung measurement on the Large Helical Device Phys. Plasmas 11 (2004) 1920–1930.